THE JOURNAL OF PHYSICAL CHEMISTRY B
A JOURNAL OF THE AMERICAN CHEMICAL SOCIETY

pubs.acs.org/JPCB

Article

Charge Inversion in 1:1 Electrolytes: Analyzing the Energetics

Nathalia Salles Vernin,* Elvis do Amaral Soares, Frederico W. Tavares, and Dirk Gillespie*

Cite This: https://doi.org/10.1021/acs.jpcb.3c00436

Read Online

ACCESS | Metrics & More | Article Recommendations | Supporting Information

ABSTRACT: The effects of bulk concentration, surface charge density, ionic diameter, and bulk dielectric constant on charge inversion in 1:1 electrolyte systems are investigated. The framework of the classical density functional theory is used to describe the mean electrostatic potential and the volume and electrostatic correlations, which combine to define the adsorption of ions at a positively charged surface. Our results show that a decrease in the dielectric constant, in particular, creates charge inversion for 1:1 electrolytes by amplifying both the electrostatic potential and the screening component (which is generally much larger than the excluded-volume component). Local electrical potential inversion can occur even for moderate concentrations and surface charges. These findings are especially significant for ionic liquids and systems with organic molecules as solvents, as these generally have a dielectric constant much smaller than water.

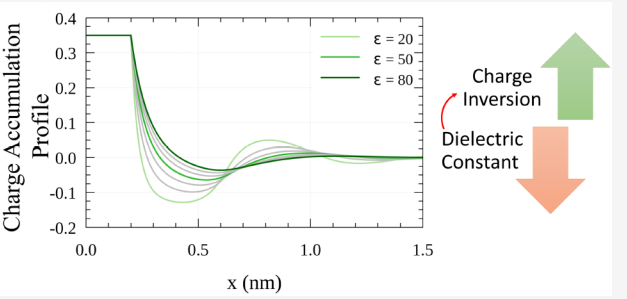

INTRODUCTION

Electrolyte systems and processes involving charges are ubiquitous, making the study of electrostatic phenomena fundamental to understanding biological, chemical, and physical processes, especially near interfaces.[1,2] Knowledge of the microscopic structure of the electrical double layer (EDL) at these interfaces is essential to understanding phenomena such as charge reversal, also known as charge inversion, where the charge on a surface undergoes an apparent inversion in sign due to a co-ion buildup.[3−5] Usually, this phenomenon is associated with an electrostatic potential inversion (i.e., a change of sign in the electrostatic potential) and directly affects the adsorption and other interfacial properties.

Charge inversion is associated with the manipulation of charged micelles, dendrimers, lipid membranes, and polyelectrolytes such as DNA and proteins.[2−4,6] For example, DNA can abruptly coagulate in the presence of macroions, such as spermine, at a critical concentration, to form large bundles. At a concentration higher than this, DNA can denature back.[6] Moreover, DNA is organized in chromatin due to the presence of histones that have a large positive charge. This complex is disassembled in the presence of electrolytes.

Another interesting situation involving overcharging is complexes formed by a charged polymer and oppositely charged particles. Examples include histone octamers forming 10 nm chromatin fiber with DNA[6] and the adsorption of albumin on strongly negatively charged polystyrene.[3] Overcharging can also be manifested in the case of attraction of like charges.[2,4,6]

Charge inversion is usually observed in systems containing multivalent ions, polyelectrolytes or surfactants, or when the surface is charge regulated.[3,7−15] Extensive investigations have discussed the effects of bulk concentration, ionic diameter, and surface charge density on charge inversion, especially for multivalent ions. In this case, the electrostatic correlations (specifically those beyond the mean electrostatic potential) play an important role. Specifically, these correlations increase the population of co-ions in the second layer because of the strongly attractive potential they create near the interface. Because these electrostatic correlations are approximately proportional to the square of the ion valence, they have a disproportionate effect in electrolytes with multivalent ions.[7−9]

Different levels of theories can be used to investigate charge inversion, including molecular simulation,[13,16−18] integral equation,[19] modified Poisson−Boltzmann equation,[14,15] and classical density functional theory (DFT).[7,8,10−13,20] With DFT, integral equations, or the modified Poisson−Boltzmann equation, it is possible to investigate the contribution of each energetic term to the charge inversion. While possible in Monte Carlo simulations,[21] it is not straightforward. Generally, the theories underlying DFT and integral equations to account for ion size and electrostatic correlations are robust and well-tested.

In a recent systematic analysis using DFT, Voukadinova and Gillespie[8] described the balance of energies at the EDL interface, how these energies change with system parameters (e.g., bulk ion concentrations, ion diameter), and how charge

Received: January 18, 2023
Revised: March 24, 2023

inversion comes about. To summarize, a change in the sign of the electrostatic potential (their metric of charge inversion) occurs when the energy due to electrostatic correlations beyond the mean-field becomes strongly negative (relative to the bath). This makes co-ion adsorption favorable and can locally change the sign of the electrostatic potential. Bulk ion concentrations and ion diameters affected the onset of charge inversion because the balance of the electrostatic correlation energy with other terms (which are discussed in the Results and Discussion) changes with these system parameters. Specifically, bulk ion concentration, ρ_i^b, did not affect the electrostatic correlation energy, but it did substantially change

$$E_i(\mathbf{x}) = \ln\left(\frac{\rho_i(\mathbf{x})}{\rho_i^b}\right) \tag{1}$$

the adsorption free energy of species i. Here, $\rho_i(\mathbf{x})$ is the concentration profile of ion species i. On the other hand, ion diameters substantially affected the electrostatic correlation energy while not changing the adsorption free energy. Specifically, large counterions produced a more negative electrostatic correlation energy at the contact distance. Here, we expand these principles to understand charge inversion in 1:1 electrolytes, which was not discussed by Voukadinova and Gillespie.[8]

Recently, Guerrero-García[19] discussed local charge inversion in concentrated 1:1 electrolyte systems using Monte Carlo and integral equation theory in the Hypernetted chain/Mean spherical approximation (HNC/MSA) approach. The charged interface was on a uniformly charged spherical colloidal particle, with diameters varying from 4 to 8 nm, immersed in an aqueous electrolyte solution. The solvent was treated implicitly as a continuum whose characteristics were described by a dielectric constant (with value 78.0). Charge inversion was attributed to the volume and electrostatic correlations.[19]

Evidence of the dielectric constant's role in the screening and overcharging of electrolyte systems has been highlighted over the years. Measures of force as a function of the distance between a silica bead and an amine-terminated surface immersed into a mixture containing multivalent ions revealed that decreasing the dielectric constant decreases the charge-inversion concentration.[22] From data of force between mica plates across a 2 M solution of 1-butyl-1-methylpyrrolidinium bis[(trifuoromethyl)sulfonyl]imide in different solvents, the screening length for each system was computed and plotted as a function of Bjerrum length.[23] It revealed a long screening length in concentrated electrolytes which increases linearly with the Bjerrum length, a phenomenon known as under-screening. The solvents analyzed have dielectric constants ranging from 22.8 to 64.

The EDL formed close to charged interfaces in systems with organic ions has also been investigated.[16,20,24,25] Goodwin and Kornyshev[24] suggested that overscreening can be important in explaining the shape of differential capacitance curves for 1:1 room-temperature ionic liquids. For concentrated systems with a dielectric constant of less than 10 composed of tetrabutylammonium and tetraphenylborate ions dissolved in dichloromethane, an oscillatory behavior was observed in the charge compensation profile obtained using molecular dynamics simulation.[16] Similar behavior was described for a system containing 1-butyl-3-methylimidazolium and tetrafluoroborate, especially near surfaces highly charged.[25,26] In the presence of acetonitrile, the oscillation magnitude of the charge compensation decreases.[25] Moreover, a dipolar shell theory was proposed by De Souza, Kornyshev, and Bazant[20] to take into account the anisotropic static dielectric tensor and qualitatively reproduce the overscreening observed in the molecular simulation of confined liquids.

While the influence of concentration and surface charge density on charge inversion in 1:1 electrolyte systems has been previously investigated,[18,19,27,28] here, we focus on the influence of the dielectric constant in amplifying the phenomenon. We do this by performing a systematic study, comprehensively varying numerous parameters to wholly understand how charge inversion is defined by the dielectric constant.

THEORY

We use DFT, which is based on the Hohenberg−Kohn theorem and statistical mechanics, to compute the profiles of ionic density $\rho_i(x)$ of the ith species, the mean electrostatic potential $\psi(x)$, and the first-order direct correlation functions $c_i^{(1)}(x)$. According to DFT, the grand potential Ω may be expressed as[29]

$$\Omega[\{\rho_k(\mathbf{x})\}] = F[\{\rho_k(\mathbf{x})\}] + \sum_i \int d\mathbf{x}\rho_i(\mathbf{x})[V_i^{\text{ext}}(\mathbf{x}) - \mu_i^{\text{b}}] \tag{2}$$

where V_i^{ext} is the nonelectrostatic external potential of species i and μ_i^{b} is the bulk chemical potential of i. $F[\{\rho_k(\mathbf{x})\}]$ is the intrinsic Helmholtz energy functional, which can be split into the ideal-gas part F^{id} and the excess part F^{ex} that includes contributions from ion volume and electrostatic correlations and direct Coulomb interactions.

The intrinsic Helmholtz energy functional due to the ideal gas is given by

$$\beta F^{\text{id}}[\{\rho_k(\mathbf{x})\}] = \sum_i \int d\mathbf{x}\rho_i(\mathbf{x})[\ln(\rho_i(\mathbf{x})\Lambda_i^3) - 1] \tag{3}$$

and depends only on the local density of the species. Here, $\beta = (k_{\text{B}}T)^{-1}$, k_{B} is the Boltzmann constant, T is the temperature, and Λ_i is the thermal de Broglie wavelength of the ith species.

With the fundamental measure theory (FMT), the Helmholtz energy functional due to the hard-sphere exclusion volume can be described by

$$\beta F^{\text{hs}}[\{\rho_k(\mathbf{x})\}] = \int d\mathbf{x}\Phi^{\text{hs}}(\{n_\alpha(\mathbf{x})\}) \tag{4}$$

where Φ^{hs} is the reduced Helmholtz energy density and $\{n_\alpha(\mathbf{x})\}$ is the set of the weighted densities for the n-component mixture given by

$$n_\alpha(\mathbf{x}) = \sum_i \int d\mathbf{x}'\rho_i(\mathbf{x}')\omega_i^{(\alpha)}(\mathbf{x} - \mathbf{x}') \tag{5}$$

The weight functions $\omega_i^{(\alpha)}(\mathbf{x})$ are related to the fundamental geometric measures of hard spheres and the expressions can be found in ref 30. The hard-sphere contribution to the first-order direct correlation function is equal to

https://doi.org/10.1021/acs.jpcb.3c00436
J. Phys. Chem. B XXXX, XXX, XXX−XXX

$$c_i^{(1),\mathrm{hs}}(\mathbf{x}) = -\frac{\delta\beta F^{\mathrm{hs}}[\Phi^{\mathrm{hs}}(\{n_\alpha\})]}{\delta\rho_i(\mathbf{x})} = -\sum_\alpha \int \mathrm{d}\mathbf{x}' \frac{\partial\Phi^{\mathrm{hs}}(\{n_\alpha\})}{\partial n_\alpha}\omega_i^{(\alpha)}(\mathbf{x}' - \mathbf{x}) \tag{6}$$

Here, we use the White Bear version of the FMT to describe the excess free energy density, Φ^{hs}.[31]

The Helmholtz energy functional due to the mean-field Coulomb interaction can be written as

$$\beta F^{\mathrm{C}}[\{\rho_k(\mathbf{x})\}] = \frac{\lambda_{\mathrm{B}}}{2}\sum_{i,j}\int \mathrm{d}\mathbf{x}' \int \mathrm{d}\mathbf{x} \frac{z_i z_j \rho_i(\mathbf{x})\rho_j(\mathbf{x}')}{|\mathbf{x} - \mathbf{x}'|} \tag{7}$$

where λ_{B} is the Bjerrum length and z_i is the valence of the ith species.

The functionalized mean-spherical approximation (fMSA) was applied to take into account the electrostatic correlation contribution to the Helmholtz energy:[32]

$$\beta F^{\mathrm{ec}}[\{\rho_k(\mathbf{x})\}] = \int \mathrm{d}\mathbf{x}\Phi^{\mathrm{MSA}}(\{q_k^{(0)}(\mathbf{x})\}) - \frac{1}{2}\sum_{i,j}\int \mathrm{d}\mathbf{x}\int \mathrm{d}\mathbf{x}'\rho_i(\mathbf{x})\rho_j(\mathbf{x}')c_{ij}^{(2),\mathrm{ec}}(\mathbf{x} - \mathbf{x}') \tag{8}$$

where the weighted density $q_i^{(0)}$ is equal to

$$q_i^{(0)} = \int \mathrm{d}\mathbf{x}'\rho_i(\mathbf{x}')\omega_i^{\mathrm{fMSA}}(\mathbf{x} - \mathbf{x}') \tag{9}$$

in which

$$\omega_i^{\mathrm{fMSA}}(\mathbf{x}) = \frac{\delta(b_i - |\mathbf{x}|)}{4\pi b_i^2} \tag{10}$$

the shell radius is $b_i = R_i + \frac{1}{2\Gamma_b}$, δ is the Dirac-delta function, R_i is the radius of the hard-spheres, and Γ_b is the MSA screening parameter computed from the bulk densities.[33] It was previously shown that the fMSA accurately produces charge inversion.[7]

The reduced Helmholtz energy density due to MSA, considering the set of weighted densities, is given by[32]

$$\Phi^{\mathrm{MSA}}(\{q_k^{(0)}\}) = -\lambda_{\mathrm{B}}\sum_i q_i^{(0)}(\mathbf{x})\frac{z_i^2\Gamma(\{q_k^{(0)}\}) + z_i\sigma_i\eta(\{q_k^{(0)}\})}{1 + \Gamma(\{q_k^{(0)}\})\sigma_i} + \frac{\Gamma(\{q_k^{(0)}\})^3}{3\pi} \tag{11}$$

where σ_i is the diameter of the species i and the expression for η can be found in refs 32 and 33. The second-order direct correlation function is from the MSA,[33] with

$$c_{ij}^{(2),\mathrm{ec}}(\mathbf{x}) = \frac{\lambda_{\mathrm{B}} z_i z_j}{4 b_i b_j}\frac{(|\mathbf{x}| - b_{ij})^2}{|\mathbf{x}|}\theta(R_{ij} - |\mathbf{x}|) \tag{12}$$

where $R_{ij} = R_i + R_j$, $b_{ij} = b_i + b_j$, and θ is the Heaviside step function.

Therefore, the electrostatic correlation contribution to the first-order direct correlation function is equal to

$$c_i^{(1),\mathrm{ec}}(\mathbf{x}) = -\beta\int \mathrm{d}\mathbf{x}'\mu_i^{\mathrm{MSA}}(\{q_k^{(0)}\})\omega_i^{\mathrm{fMSA}}(\mathbf{x} - \mathbf{x}') + \sum_j \int \mathrm{d}\mathbf{x}' c_{ij}^{(2),\mathrm{ec}}(\mathbf{x} - \mathbf{x}') \tag{13}$$

At thermodynamic equilibrium, the density profiles are given by

$$\rho_i(\mathbf{x}) = \rho_i^{\mathrm{b}}\exp[E_i(\mathbf{x})] \tag{14}$$

where the adsorption free energy written in terms of first-order direct correlation functions is

$$E_i(\mathbf{x}) = \Delta c_i^{(1),\mathrm{ec}}(\mathbf{x}) + \Delta c_i^{(1),\mathrm{hs}}(\mathbf{x}) - \beta z_i e\psi(\mathbf{x}) - \beta V_i^{\mathrm{ext}}(\mathbf{x}) \tag{15}$$

Here, e is the fundamental charge. The superscripts hs and ec refer to hard-sphere and electrostatic correlation contributions, respectively. $\Delta c_i^{(1)}$ is defined by

$$\Delta c_i^{(1)}(\mathbf{x}) = \beta\mu_i^{\mathrm{b,ex}} + c_i^{(1)}(\mathbf{x}) \equiv \beta\mu_i^{\mathrm{b,ex}} - \beta\frac{\delta F^{\mathrm{ex}}[\{\rho_k(\mathbf{x})\}]}{\delta\rho_i(\mathbf{x})} \tag{16}$$

Here, $\mu^{\mathrm{b,ex}}$ is the excess chemical potential at bulk reservoir of the ionic species i.

The mean electrostatic potential $\psi(\mathbf{x})$ is defined by the Poisson equation,

$$-\varepsilon\varepsilon_0\nabla^2\psi(\mathbf{x}) = e\sum_i \rho_i(\mathbf{x}) \tag{17}$$

where ε is the dielectric coefficient (assumed constant throughout the system) and ε_0 is the permittivity of free space. Neumann boundary condition was applied at the surface and a distance far from the surface.[34] Importantly for our purposes, we note that both $\psi(\mathbf{x})$ and $\Delta c_i^{(1),\mathrm{ec}}(\mathbf{x})$ are inversely proportional to ε. Specifically, both are proportional to the Bjerrum length λ_{B}; that is,

$$e\beta\psi(\mathbf{x}) \propto \frac{\beta e^2}{4\pi\varepsilon\varepsilon_0} = \lambda_{\mathrm{B}} \tag{18}$$

and[32]

$$\Delta c_i^{(1),\mathrm{ec}}(\mathbf{x}) \propto \frac{\beta e^2}{4\pi\varepsilon\varepsilon_0} = \lambda_{\mathrm{B}} \tag{19}$$

No other terms (e.g., $\Delta c_i^{(1),\mathrm{hs}}(\mathbf{x})$ or $V_i^{\mathrm{ext}}(\mathbf{x})$) depend on ε. Therefore, decreasing ε will amplify only the two electrostatic terms.

Moreover, we considered a single, smooth, hard wall with uniform surface charge density σ located at $x = 0$. Therefore, all density and electrostatic profiles vary only in the x-direction (and are constant parallel to the wall). Ions are charged hard spheres, and the solvent is implicit, present only in the form of the dielectric constant.

The charge accumulation as a function of the distance apart from the surface is defined by

$$Q(x) = e\sum_i \int_0^x \mathrm{d}x' z_i\rho_i(x') + \sigma \tag{20}$$

where σ is the surface charge density.

https://doi.org/10.1021/acs.jpcb.3c00436
J. Phys. Chem. B XXXX, XXX, XXX−XXX

RESULTS AND DISCUSSION

Torrie and Valleau,[18] using Monte Carlo, reported the charge inversion phenomenon for a 1:1 symmetrical electrolyte system with bulk concentration and ionic diameters of 2 M and 0.425 nm, respectively, close to a charged wall with surface charge density of 0.35 C/m^2. Our DFT calculations reproduce the Monte Carlo data of Torrie and Valleau[18] (Figure 1A) and predict the overcompensation of the surface charge at $x \approx 0.8$ nm. That is, at that distance from the wall, the counterion and co-ion profiles intersect, as shown in Figure 1A; to the left of that intersection, the local space charge is negative (due to the counterions), and to the right, it is positive (the co-ions are at a higher concentration than the counterions) until the counterion and co-ion concentrations become the same in the bulk. Figure 1B presents the anion first-order direct correlation functions due to volume and electrostatic correlations, the mean electrostatic potential, and the adsorption free energy profiles.

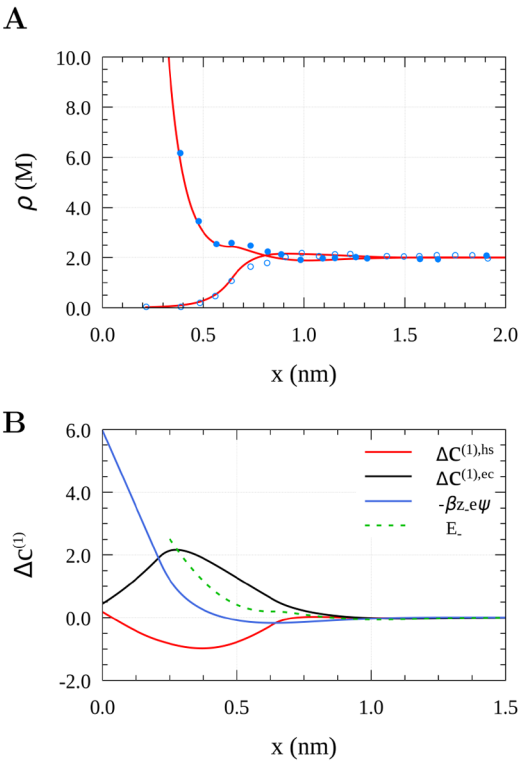

Figure 1. (A) Ionic density profile. (B) Anion first-order direct correlation function, mean electrostatic potential, and adsorption free energy of an aqueous system with 1:1 symmetrical electrolyte with a bulk concentration of 2 M. The surface charge density is 0.35 C/m^2. Ionic diameters are 0.425 nm, temperature is 298.15 K, and ε = 78.5. Circles are Monte Carlo data from ref 18.

$\Delta c^{(1),\mathrm{hs}}(x)$ measures how favorable it is to insert an uncharged sphere of the same size as the ion from the bulk solution to a distance x away from the surface, while $\Delta c^{(1),\mathrm{ec}}(x)$ measures the screening capability of the ions (i.e., how strong the anion attraction is with respect to the cations around it).[8] The mean electrostatic potential $\psi(x)$ is related to the counterions' ability, in this case, the anion, to screen the surface charge. The adsorption free energy profile has a discontinuity due to the external potential, which is zero for x greater than or equal to the radius of the ions and infinite otherwise (Figure 1B).

In Figure 1B, there is a potential inversion around 0.45 nm. This is compensated by the electrostatic correlation, so that the ion profiles' crossover does not occur here. However, moving away from the surface, the electrostatic correlation becomes weaker while the electrostatic potential remains negative, producing a slight decrease of the counterion concentration below the bulk concentration (Figure 1A).

As shown in Figure 2, for an aqueous system with a 1:1 symmetrical electrolyte with diameter of 0.4 nm, the EDL contracts as the bulk concentration increases. Moreover, there is a drop in the surface electrostatic potential for highly concentrated systems. This is because the electrical work to bring an anionic point charge from the bulk solution to the wall against the force exerted by the electric field is smaller than for less concentrated systems (Figure S1). Overall, an increase in the bulk concentration, in addition to favoring the occurrence of charge inversion (as previously described[8]), moves the phenomenon closer to the wall (Figure 3); that is, for more concentrated systems, the co-ion density (Figure 2B) exceeds the counterion density (Figure 2A) closer to the surface, and the electrostatic potential changes sign closer to the surface as well (Figure S1A).

The magnitude of the 1:1 electrolyte charge inversion is also more pronounced with an increase in ionic diameter (Figures 4 and 5), as was previously described for multivalent electro-

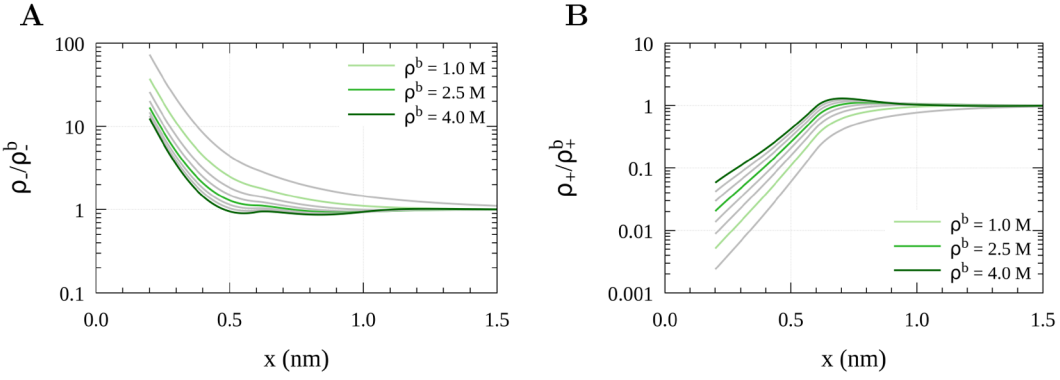

Figure 2. Counterion (A) and co-ion (B) density profiles of an aqueous system with 1:1 symmetrical electrolyte close to a charged wall with surface charge density of 0.35 C/m^2 for different bulk concentrations. Diameters are 0.4 nm, temperature is 298.15 K, and ε = 78.5. Three concentrations are shown in color, and intermediate ones are shown in gray.

https://doi.org/10.1021/acs.jpcb.3c00436
J. Phys. Chem. B XXXX, XXX, XXX−XXX

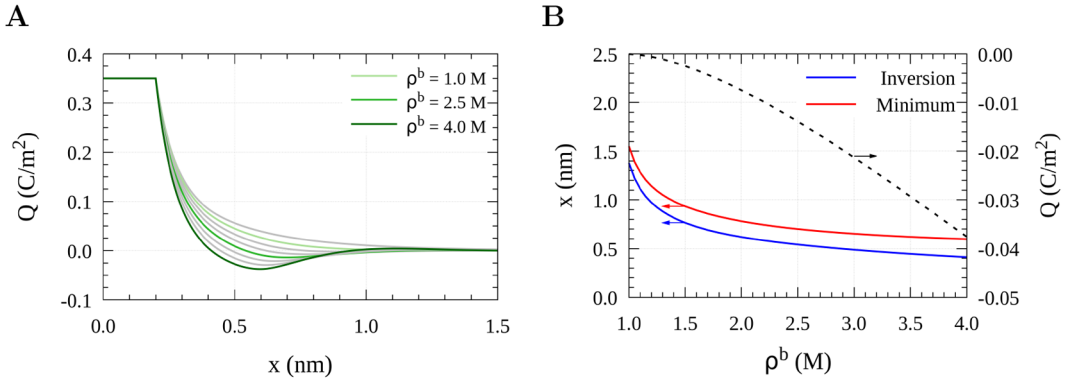

Figure 3. Charge accumulation profile (A) and position and magnitude of charge inversion as a function of bulk density (B) for an aqueous system with 1:1 symmetrical electrolyte close to a charged wall with surface charge density of 0.35 C/m^2 for different bulk concentrations. Diameters are 0.4 nm, temperature is 298.15 K, and ε = 78.5. Three concentrations are shown in color, and intermediate ones are shown in gray. The blue line represents the position of the charge inversion; specifically, it is the position where the first change in the sign of the charge accumulation profile happens. The red line refers to the position of the minimum charge accumulation profile. The magnitude of this minimum point is represented by the black line (y-axis on the right). The arrows indicate which y-axis is used for that curve.

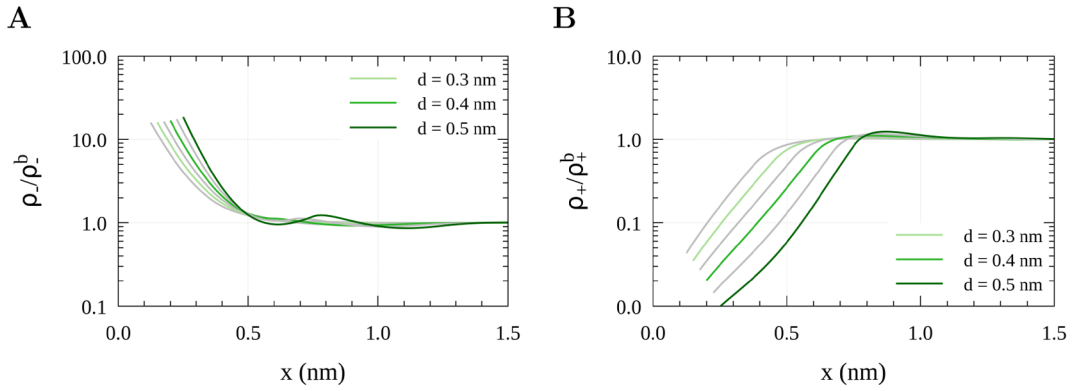

Figure 4. Counterion (A) and co-ion (B) density profiles of an aqueous system with 1:1 symmetrical electrolyte close to a charged wall with surface charge density of 0.35 C/m^2 for different ion diameters. Bulk concentration is 2.5 M, temperature is 298.15 K, and ε = 78.5. Three diameters are shown in color and intermediate ones are shown in gray.

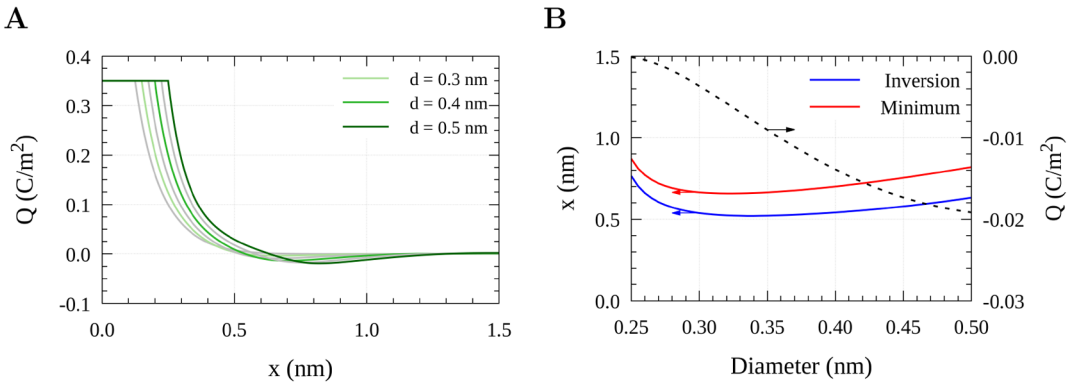

Figure 5. Charge accumulation profile (A) and position and magnitude of charge inversion as a function of bulk density (B) for an aqueous system with 1:1 symmetrical electrolyte close to a charged wall with surface charge density of 0.35 C/m^2 for different ion diameters. Bulk concentration is 2.5 M, temperature is 298.15 K, and ε = 78.5. Three diameters are shown in color, and intermediate ones are shown in gray on the left. The blue line represents the position of the charge inversion, whereas the red line refers to the position of the minimum charge accumulation profile. The magnitude of this minimum point is represented by the black line (y-axis on the right). The arrows indicate which y-axis is used for that curve.

lytes.[8] Figure 5 shows that, with increasing diameter, initially the position of the charge inversion decreases before reaching a minimum, followed by an increase. This is due to ion layering. For larger diameters, it is possible to observe a multilayer ordering in highly concentrated systems. There is an increase in the surface electrostatic potential value with an increment of the ionic diameter (Figure S2A) due to the external potential not allowing any ion at a position smaller than its radius.

With an increase in the ion size, the maximum and minimum values of $\Delta c^{(1),ec}$ become more pronounced (Figure S2B). This

https://doi.org/10.1021/acs.jpcb.3c00436
J. Phys. Chem. B XXXX, XXX, XXX−XXX

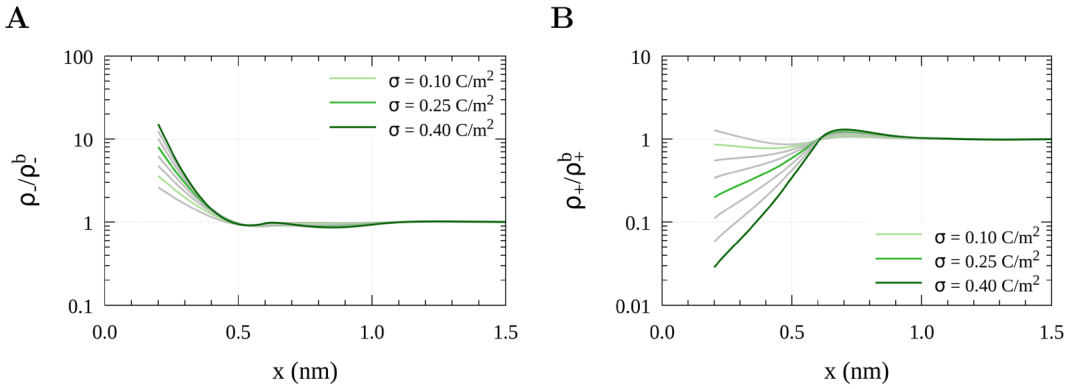

Figure 6. Counterion (A) and co-ion (B) density profiles of an aqueous system with 1:1 symmetrical electrolyte close to a charged wall with different surface charge densities. Diameters are 0.4 nm, bulk concentration is 4.0 M, temperature is 298.15 K, and ε = 78.5. Three surface charges are shown in color, and intermediate ones are shown in gray.

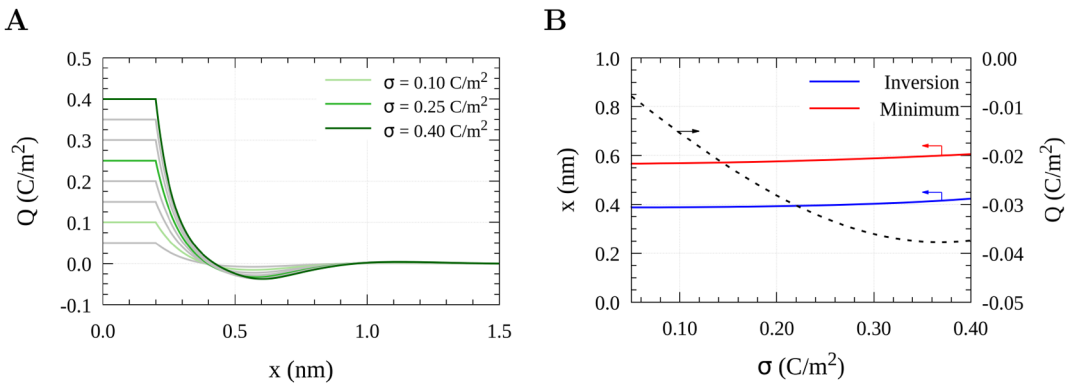

Figure 7. Charge accumulation profile (A) and position and magnitude of charge inversion as a function of bulk density (B) for an aqueous system with 1:1 symmetrical electrolyte close to a charged wall with surface charge density of 0.35 C/m^2 for different surface charge densities. Diameters are 0.4 nm, temperature is 298.15 K, and ε = 78.5. Three concentrations are shown in color, and intermediate ones are shown in gray. The blue line represents the position of the charge inversion, whereas the red line refers to the position of the minimum charge accumulation profile. The magnitude of this minimum point is represented by the black line (y-axis on the right). The arrows indicate which y-axis is used for that curve.

contribution is essential to promoting charge inversion. Regarding $\Delta c^{(1),hs}$, steric correlations dominate for bigger diameters (see Figure S2C and the discussion by Voukadinova and Gillespie[8]).

When increasing the surface charge density, there is a tendency to form a counterion layer near the wall that overcompensates the surface charge, leading to charge inversion (Figures 6 and 7). The position of charge inversion is nearly constant with increasing surface charge density, whereas the magnitude of charge inversion increases (Figure 7). The potential inversion is more pronounced with an increase in the surface charge density (Figure S3A). This is because the increased surface charge increases the attractive screening component significantly more than the repulsive hard-sphere component (Figure S3).

Therefore, 1:1 electrolyte charge inversion is also associated with high concentrations, high surface charges, and/or big ions for the same reasons described by Voukadinova and Gillespie[8] for multivalent electrolytes. Next, we focus on a new aspect not considered before (to our knowledge): the dielectric constant.

Effect of Dielectric Constant. To investigate the main contributions of the dielectric constant to overcharging, we varied this parameter from 20 to 80 for 1:1 symmetrical electrolyte systems. A dielectric constant of around 20 occurs in ionic liquid systems. We kept the surface charge constant at 0.35 C/m^2 in all the cases presented here. In the Supporting Information, the profiles for a range of surface charge densities varying from 0.05 to 0.40 C/m^2 can be found (Figures S4 and S15).

In Figure 8, the ion concentration profiles and the three main counterion energetic components are shown for a bulk concentration of 4.0 M. The decrease in the medium's dielectric constant amplifies the surface's electrical field to create a more pronounced potential inversion, as shown in Figure 8A. Moreover, there is an increase in the surface electrostatic potential for systems with smaller permittivity and high bulk concentration. This is because the work to bring an anionic point charge from the bulk solution to the wall against the force exerted by the electric field increases with a decreasing dielectric constant. The same trend can be seen for an increase in the surface charge density, as shown in Figure S4. However, at high surface charges for concentrated systems with big ions, the minimum in the electrostatic potential can shrink due to the repulsive potential of the steric component as the first ion layer becomes extremely crowded.[8]

The amplification of the electric field produced by the counterions as a consequence of the decrease in the dielectric constant also significantly affects the screening capability of ions. With the decrease of permittivity, the maximum and minimum peaks of $\Delta c^{(1),ec}$ become more pronounced as shown by Figure 8B. These maxima draw in more counterions at low dielectric constants than at high ones (Figure 8F). This is not

https://doi.org/10.1021/acs.jpcb.3c00436
J. Phys. Chem. B XXXX, XXX, XXX−XXX

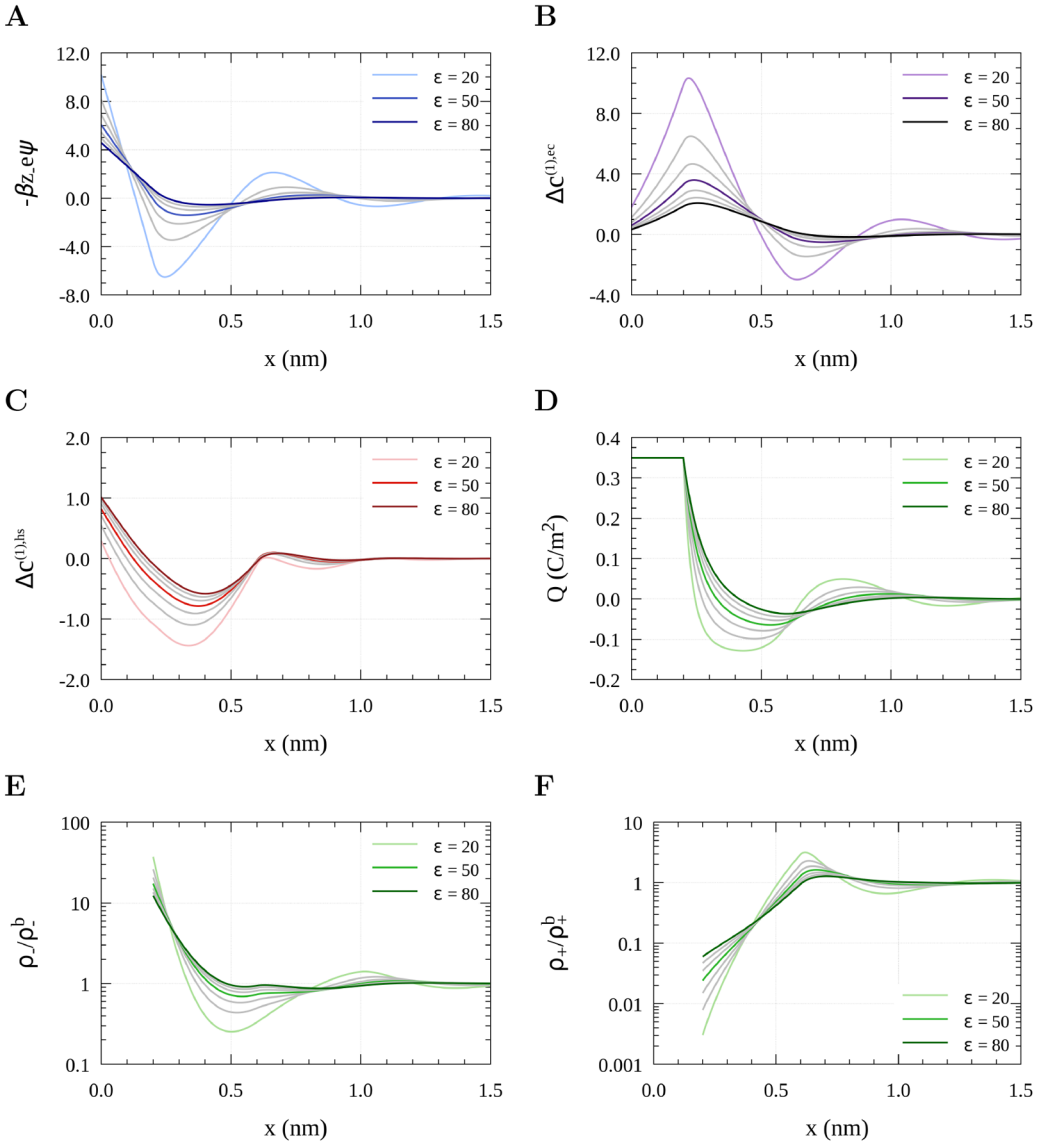

Figure 8. Mean electrostatic potential (A), anion first-order direct correlation function due to electrostatic correlation (B) and volume exclusion (C), charge accumulation profile (D), and counterion (E) and co-ion (F) density profiles of an aqueous system with 1:1 symmetrical electrolyte close to a charged wall with surface charge density of 0.35 C/m^2 and bulk concentration of 4.0 M for different dielectric constants. Diameters are 0.4 nm, and the temperature is 298.15 K. Three dielectric constant values are shown in color, and intermediate ones are shown in gray.

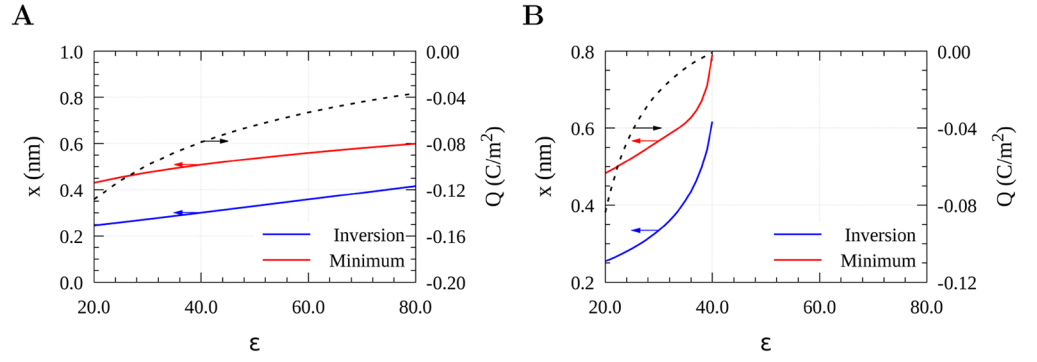

Figure 9. Charge accumulation profile for aqueous systems with 1:1 symmetrical electrolyte close to a charged wall with surface charge density of 0.35 C/m^2 for different dielectric constants. Bulk concentrations are 4.0 M (A) and 0.1 M (B). Diameters are 0.4 nm, and temperature is 298.15 K. The blue line represents the position of the charge inversion, whereas the red line refers to the position of the minimum charge accumulation profile. The magnitude of this minimum point is represented by the black line (*y*-axis on the right). The arrows indicate which *y*-axis is used for that curve.

https://doi.org/10.1021/acs.jpcb.3c00436
J. Phys. Chem. B XXXX, XXX, XXX−XXX

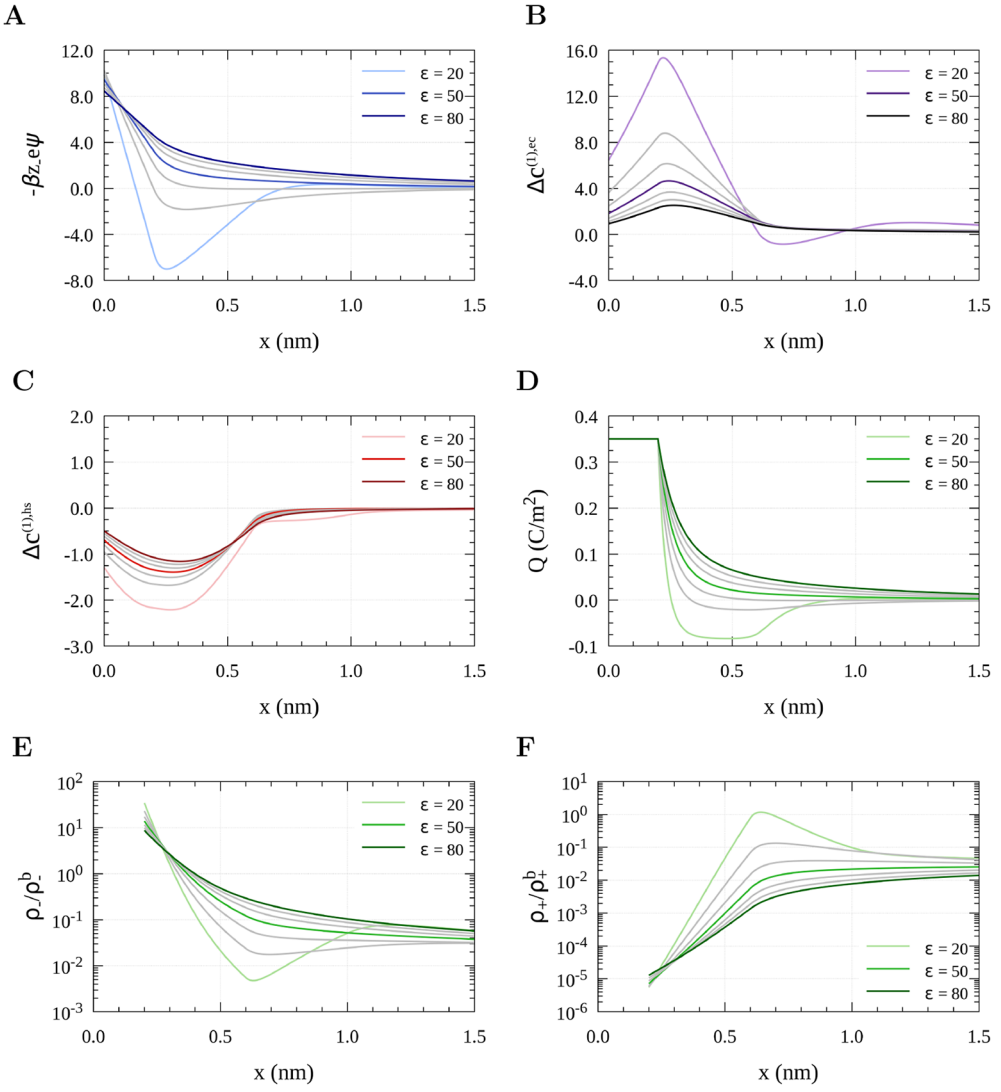

Figure 10. Mean electrostatic potential (A), anion first-order direct correlation function due to electrostatic correlation (B) and volume exclusion (C), charge accumulation profile (D), and counterion (E) and co-ion (F) density profiles of an aqueous system with 1:1 symmetrical electrolyte close to a charged wall with surface charge density of 0.35 C/m^2 and bulk concentration of 0.1 M for different dielectric constants. Diameters are 0.4 nm, and the temperature is 298.15 K. Three dielectric constant values are shown in color, and intermediate ones are shown in gray.

only because these maxima near the wall grow with decreasing dielectric constant but also because that growth is faster than growth of the repulsive energies due to excluded volume correlations (Figure 8C).

Overall, these results show that charge inversion is very sensitive to decreases in dielectric constant, and a decrease amplifies charge inversion (black dashed lines in Figure 9). As we see below, this reduces the need for other charge inversion-promoting parameters (e.g., large bulk ion concentrations, ion diameters, and surface charge) to induce charge inversion.

Generally, charge inversion is associated with high concentrations, especially for 1:1 electrolytes. However, at low dielectric constant, charge inversion also happens for systems with moderate concentrations, as shown in Figures 10 and S10−S15. Charge inversion is present for ε = 20 but not for ε = 80 for a bulk concentration of 0.1 M (Figure 9B). In fact, for 1:1 symmetrical electrolyte solution at 0.1 M with an ion diameter of 0.4 nm near a charged wall with a surface charge density of 0.35 C/m^2, there is no charge inversion if the dielectric constant is greater than 40.

The same low-dielectric amplification can also be seen for moderate surface charge density (Figure S10); charge inversion is usually associated with large surface charge. Interestingly, the surface electrostatic potential for ε = 20 is smaller than for ε = 30 (Figure 10A). This counterintuitive effect is mainly due to the electrostatic correlation (Figure 10B), and it is contrary to the trend observed by the classical Poisson−Boltzmann equation, which does not include any of the ionic correlations we include with DFT.

Ideally, one would like to have a simple scaling theory that ties together all the system parameters to better define how the dielectric constant amplifies charge inversion. Besteman et al.[22] suggested such a theory based on the bulk concentration needed to first achieve charge inversion. They approximately measured this concentration with their atomic force spectroscopy experiments, and those data fit their theory that the change inversion onset bulk concentration c_0 is given by

$$c_0 = \left|\frac{\sigma}{2Rze}\right| \exp[\mu_c(\Gamma')] \exp(\beta\Delta\mu^h) \tag{21}$$

https://doi.org/10.1021/acs.jpcb.3c00436
J. Phys. Chem. B XXXX, XXX, XXX−XXX

with

$$\mu_c(\Gamma') = -\beta^{-1}(1.65\Gamma' - 2.61\Gamma'^{1/4} + 0.26\ln\Gamma' + 1.95) \quad (22)$$

and

$$\Gamma' = \frac{\beta}{4\varepsilon\varepsilon_0}\left|\frac{e^3z^3\sigma}{\pi}\right|^{1/2} \quad (23)$$

Here, $\Delta\mu^h$ refers to hydration and binding contributions, and $\mu_c(\Gamma')$ "accounts for spatial interactions between multivalent ions", meaning that it includes all the ionic correlations that we compute with DFT. Moreover, these correlations are encapsulated into the scaling parameter Γ'. It is beyond the scope of this work to test this theory, but Γ' does not include ion size effects, as there are no ion sizes in eqs 22 and 23; it only appears in eq 21 represented by the radius R. Even neglecting those (which one should not[8]) in DFT, $\Delta c^{(1),ec}$ does not scale as $z^{3/2}/\varepsilon$.[32] Therefore, a different scaling theory of charge inversion (and how it relates to the forces between two walls that Besteman et al.[22] measured) is probably needed. This may be addressed in future work.

CONCLUSIONS

The energetics of charge inversion in 1:1 hard-sphere electrolytes was analyzed. Previously, analysis of how charge inversion occurs focused on electrolytes with multivalent ions (e.g., ref 8). Here, we found that charge inversion in 1:1 electrolytes stems from the same shifting of energetic components that make up the electrochemical potential that was found in multivalent systems. Specifically, the electrostatic correlations beyond the mean-field create a favorable environment for co-ions to accumulate in the second layer of the EDL when the surface charge is large, ion concentrations are high, or counterions are large. Moreover, this energy well (with respect to the bath) can become so pronounced that the electrostatic potential changes sign.

New in our analysis was the role of the dielectric constant ε. We found that a low dielectric constant is a substantial driver and amplifier of charge inversion in 1:1 electrolytes. This is because both electrostatic terms (i.e., the mean electrostatic potential and the electrostatic correlations beyond the mean-field) are inversely proportional to ε. Lowering the dielectric constant (e.g., to the value of ionic liquids) then increases the role of these terms. Charge inversion is amplified (compared to high dielectric aqueous electrolytes) because electrostatic correlations, the energy component that creates charge inversion in the first place, are larger.

The results here are significant for real-world systems such as room-temperature ionic liquids and electrolytes in organic solvents. With their low dielectric constants, our results indicate that charge inversion ought to be significantly more prevalent in those systems than in aqueous ones. This is important not only for the basic understanding of charge inversion in experiments (e.g., using a new current monitoring technique[35]) but also for harnessing charge inversion for technological applications (e.g., ref 36).

For future extensions of this work, we note that the charge inversion reported here could be even more pronounced if a surface with discrete charges was used, similar to the work of Wang and Wu[17] for a 3:1 electrolyte solution for different dielectric constants. Moreover, charge inversion could be further impacted by using local dielectric coefficients to simulate the orientation of solvent molecules near the surface.[4,37]

ASSOCIATED CONTENT

Supporting Information

The Supporting Information is available free of charge at https://pubs.acs.org/doi/10.1021/acs.jpcb.3c00436.

Additional graphs showing the contributions of each energetic term to the charge inversion (PDF)

AUTHOR INFORMATION

Corresponding Authors

Nathalia Salles Vernin − *Department of Sanitary and Environmental Engineering, Rio de Janeiro State University, Rio de Janeiro, Rio de Janeiro 20550-900, Brazil;* orcid.org/0000-0002-3705-4884; Email: nathalia.vernin@eng.uerj.br

Dirk Gillespie − *Department of Physiology and Biophysics, Rush University Medical Center, Chicago, Illinois 60612, United States*; Email: dirk_gillespie@rush.edu

Authors

Elvis do Amaral Soares − *School of Chemistry, Federal University of Rio de Janeiro, Rio de Janeiro, Rio de Janeiro 21941-909, Brazil;* orcid.org/0000-0002-6202-9875

Frederico W. Tavares − *Chemical Engineering Program, Alberto Luiz Coimbra Institute for Graduate Studies and Research in Engineering (COPPE), Federal University of Rio de Janeiro, Rio de Janeiro, Rio de Janeiro 21941-972, Brazil; School of Chemistry, Federal University of Rio de Janeiro, Rio de Janeiro, Rio de Janeiro 21941-909, Brazil;* orcid.org/0000-0001-8108-1719

Complete contact information is available at: https://pubs.acs.org/10.1021/acs.jpcb.3c00436

Notes

The authors declare no competing financial interest.

ACKNOWLEDGMENTS

The research reported here was supported by Fulbright through the Junior Faculty Member Award, Carlos Chagas Filho Foundation for Research Support of the State of Rio de Janeiro (FAPERJ) under award numbers E-26/010.002523/2019 and SEI-260003/015556/2021 to N.S.V. This work used resources of the "Centro Nacional de Processamento de Alto Desempenho em São Paulo" (CENAPAD-SP).

REFERENCES

(1) Levin, Y. Electrostatic correlations: from plasma to biology. *Rep. Prog. Phys.* **2002**, *65*, 1577−1632.

(2) Naji, A.; Jungblut, S.; Moreira, A. G.; Netz, R. R. Electrostatic interactions in strongly coupled soft matter. *Physica A* **2005**, *352*, 131−170.

(3) de Vos, W. M.; Lindhoud, S. Overcharging and charge inversion: Finding the correct explanation(s). *Adv. Colloid Interface Sci.* **2019**, *274*, 102040.

(4) Gonella, G.; Backus, E. H.; Nagata, Y.; Bonthuis, D. J.; Loche, P.; Schlaich, A.; Netz, R. R.; Kühnle, A.; McCrum, I. T.; Koper, M. T.; et al. Water at charged interfaces. *Nature Reviews Chemistry* **2021**, *5*, 466−485.

(5) Tang, Z.; Mier-y Teran, L.; Davis, H.; Scriven, L.; White, H. Non-local free-energy density-functional theory applied to the electrical double layer. *Mol. Phys.* **1990**, *71*, 369−392.

(6) Grosberg, A. Y.; Nguyen, T. T.; Shklovskii, B. I. Colloquium: The physics of charge inversion in chemical and biological systems. *Rev. Mod. Phys.* **2002**, *74*, 329−345.
(7) Voukadinova, A.; Valiskó, M.; Gillespie, D. Assessing the accuracy of three classical density functional theories of the electrical double layer. *Phys. Rev. E* **2018**, *98*, 1−15.
(8) Voukadinova, A.; Gillespie, D. Energetics of counterion adsorption in the electrical double layer. *J. Chem. Phys.* **2019**, *150*, 154706.
(9) Lin, K.; Lin, C. Y.; Polster, J. W.; Chen, Y.; Siwy, Z. S. Charge Inversion and Calcium Gating in Mixtures of Ions in Nanopores. *J. Am. Chem. Soc.* **2020**, *142*, 2925−2934.
(10) Jiang, T.; Wu, J. Ionic effects in collapse of polyelectrolyte brushes. *J. Phys. Chem. B* **2008**, *112*, 7713−7720.
(11) Gillespie, D.; Petsev, D. N.; van Swol, F. Electric Double Layers with Surface Charge Regulation Using Density Functional Theory. *Entropy* **2020**, *22*, 132.
(12) Gillespie, D.; Khair, A. S.; Bardhan, J. P.; Pennathur, S. Efficiently accounting for ion correlations in electrokinetic nanofluidic devices using density functional theory. *J. Colloid Interface Sci.* **2011**, *359*, 520−529.
(13) Wang, L.; Liang, H.; Wu, J. Electrostatic origins of polyelectrolyte adsorption: theory and Monte Carlo simulations. *J. Chem. Phys.* **2010**, *133*, 044906.
(14) Das, T.; Bratko, D.; Bhuiyan, L. B.; Outhwaite, C. W. Polyelectrolyte solutions containing mixed valency ions in the cell model: A simulation and modified Poisson−Boltzmann study. *J. Chem. Phys.* **1997**, *107*, 9197−9207.
(15) Bhuiyan, L. B.; Outhwaite, C. W. The cylindrical electric double layer in the modified Poisson-Boltzmann theory. *Philosophical Magazine B* **1994**, *69*, 1051−1058.
(16) Bresme, F.; Robotham, O.; Chio, W. I.; Gonzalez, M. A.; Kornyshev, A. Debye screening, overscreening and specific adsorption in solutions of organic ions. *Phys. Chem. Chem. Phys.* **2018**, *20*, 27684−27693.
(17) Wang, Z. Y.; Wu, J. Ion association at discretely-charged dielectric interfaces: Giant charge inversion. *J. Chem. Phys.* **2017**, *147*, 024703.
(18) Torrie, G. M.; Valleau, J. P. Electrical double layers. I. Monte Carlo study of a uniformly charged surface. *J. Chem. Phys.* **1980**, *73*, 5807−5816.
(19) Guerrero-García, G. I. Local inversion of the mean electrostatic potential, maximum charge reversal, and capacitive compactness of concentrated 1:1 salts: The crucial role of the ionic excluded volume and ion correlations. *J. Mol. Liq.* **2022**, *361*, 119566.
(20) De Souza, J. P.; Kornyshev, A. A.; Bazant, M. Z. Polar liquids at charged interfaces: A dipolar shell theory. *J. Chem. Phys.* **2022**, *156*, 244705.
(21) Boda, D.; Giri, J.; Henderson, D.; Eisenberg, B.; Gillespie, D. Analyzing the components of the free-energy landscape in a calcium selective ion channel by Widom's particle insertion method. *J. Chem. Phys.* **2011**, *134*, 055102.
(22) Besteman, K.; Zevenbergen, M. A.; Lemay, S. G. Charge inversion by multivalent ions: Dependence on dielectric constant and surface-charge density. *Physical Review E - Statistical, Nonlinear, and Soft Matter Physics* **2005**, *72*, 061501.
(23) Lee, A. A.; Perez-Martinez, C. S.; Smith, A. M.; Perkin, S. Underscreening in concentrated electrolytes. *Faraday Discuss.* **2017**, *199*, 239−259.
(24) Goodwin, Z. A.; Kornyshev, A. A. Underscreening, overscreening and double-layer capacitance. *Electrochem. Commun.* **2017**, *82*, 129−133.
(25) Feng, G.; Huang, J.; Sumpter, B. G.; Meunier, V.; Qiao, R. A "counter-charge layer in generalized solvents" framework for electrical double layers in neat and hybrid ionic liquid electrolytes. *Phys. Chem. Chem. Phys.* **2011**, *13*, 14723−14734.
(26) Ivaništšev, V.; O'Connor, S.; Fedorov, M. V. Poly(a)morphic portrait of the electrical double layer in ionic liquids. *Electrochem. Commun.* **2014**, *48*, 61−64.
(27) Yu, Y.-X.; Wu, J.; Gao, G.-H. Density-functional theory of spherical electric double layers and ζ potentials of colloidal particles in restricted-primitive-model electrolyte solutions. *J. Chem. Phys.* **2004**, *120*, 7223−7233.
(28) Patra, C. N.; Ghosh, S. K. A nonlocal density functional theory of electric double layer: symmetric electrolytes. *J. Chem. Phys.* **1994**, *100*, 5219−5229.
(29) Evans, R. In *Fundamentals of inhomogeneous fluids*; Henderson, D., Ed.; Marcel Dekker: New York, 1992; Chapter 3, pp 85−116.
(30) Rosenfeld, Y. Free energy model for inhomogeneous fluid mixtures: Yukawa-charged hard spheres, general interactions, and plasmas. *J. Chem. Phys.* **1993**, *98*, 8126−8148.
(31) Roth, R.; Evans, R.; Lang, A.; Kahl, G. Fundamental measure theory for hard-sphere mixtures revisited: the White Bear version. *J. Phys.: Condens. Matter* **2002**, *14*, 12063−12078.
(32) Roth, R.; Gillespie, D. Shells of charge: A density functional theory for charged hard spheres. *J. Phys.: Condens. Matter* **2016**, *28*, 244006.
(33) Blum, L.; Rosenfeld, Y. Relation between the free energy and the direct correlation function in the mean spherical approximation. *J. Stat. Phys.* **1991**, *63*, 1177−1190.
(34) Barbosa, N. S. V.; Lima, E. R. A.; Boström, M.; Tavares, F. W. Membrane potential and ion partitioning in an erythrocyte using the Poisson−Boltzmann equation. *J. Phys. Chem. B* **2015**, *119*, 6379−6388.
(35) Chou, K.-H.; McCallum, C.; Gillespie, D.; Pennathur, S. An Experimental Approach to Systematically Probe Charge Inversion in Nanofluidic Channels. *Nano Lett.* **2018**, *18*, 1191−1195.
(36) Loessberg-Zahl, J.; Janssen, K. G. H.; McCallum, C.; Gillespie, D.; Pennathur, S. (Almost) Stationary Isotachophoretic Concentration Boundary in a Nanofluidic Channel Using Charge Inversion. *Anal. Chem.* **2016**, *88*, 6145−6150.
(37) Wang, X.; Liu, K.; Wu, J. Demystifying the Stern layer at a metal-electrolyte interface: Local dielectric constant, specific ion adsorption, and partial charge transfer. *J. Chem. Phys.* **2021**, *154*, 124701.

https://doi.org/10.1021/acs.jpcb.3c00436
J. Phys. Chem. B XXXX, XXX, XXX−XXX